UNIVERSIDAD DE CHILE
FACULTAD DE CIENCIAS FÍSICAS Y MATEMÁTICAS
DEPARTAMENTO DE INGENIERÍA MATEMÁTICA

ESTIMATION OF RELATIVE PRESSURE FROM VELOCITY MEASUREMENTS IN BLOOD FLOWS: STATE-OF-THE-ART AND NEW APPROACHES

TESIS PARA OPTAR AL GRADO DE MAGÍSTER EN CIENCIAS DE LA INGENIERÍA, MENCIÓN MATEMÁTICAS APLICADAS

MEMORIA PARA OPTAR AL TÍTULO DE INGENIERO CIVIL MATEMÁTICO

RODOLFO ANDRÉS NÚÑEZ URIBE

PROFESORES GUÍAS:
CRISTÓBAL BERTOGLIO BELTRÁN
AXEL OSSES ALVARADO

MIEMBROS DE LA COMISIÓN:
JOAQUÍN MURA MARDONES

SANTIAGO DE CHILE
MAYO 2016

ESTIMACIÓN DE PRESIÓN RELATIVA USANDO MEDICIONES DE VELOCIDAD EN FLUJOS SANGUINEOS: ESTADO-DEL-ARTE Y NUEVOS ENFOQUES

El gradiente de presión a lo largo de vasos sanguíneos con estenosis es un índice clínico importante para el diagnóstico de la severidad de patologías cardiovasculares. Mientras el estándar clínico para su medida es una cateterización invasiva (medir directamente la presión introduciendo un catéter en los vasos sanguíneos), la resonancia magnética de contraste de fase ha emergido como una prometedora herramienta para permitir cuantificaciones no invasivas de la presión relativa, ligando las medidas de velocidad (resueltas con alta resolución espacial) con la presión relativa vía las ecuaciones de Navier–Stokes. El objetivo de este trabajo es resumir, proponer y comparar distintos métodos de estimación de la presión relativa a través de una estenosis. Para esto usaremos simulaciones numéricas del fluido sanguíneo.

Primero resumimos los métodos actuales para estimación de presión relativa, i.e. PPE, STE y WERP. Luego de proponer algunas mejoras a estos métodos, proponemos otra familia de métodos que integran las medidas sobre un volumen de control para recuperar la presión relativa. Realizamos un estudio comparativo de los métodos existentes y de los propuestos en este trabajo usando datos sintéticos perturbados en dimensión dos.

PPE consiste en resolver un problema de Poisson para la presión p, usando medidas de velocidad de flujo sanguineo $\boldsymbol{u}$: $\boldsymbol{\nabla} p = f(\boldsymbol{u})$. STE le agrega un término de difusión a este problema, agregando una velocidad ficticia $\boldsymbol{w}$ a divergencia nula. Esto lleva a resolver en la práctica un problema de Stokes: $-\Delta \boldsymbol{w} + \boldsymbol{\nabla} p = f(\boldsymbol{u})$. Ambos enfoques entregan una estimación de la presión en todo el dominio. En este trabajo proponemos integrar por partes el lado derecho de STE, reduciéndo los ordenes de derivación de las medidas, reduciendo así la propagación del ruido presente en las mediciones. Llamaremos a este método STEint.

Por otro lado, WERP toma un enfoque distinto, en el que solo pedimos la diferencia de presión entre dos superficies basada en un balance de energía integral. Este método solo requiere calcular integrales sobre el dominio utilizando la velocidad medida. Esto lo hace muy superior en tiempo de cálculo, sin embargo, no obtenemos una estimación de la presión en todo el dominio, sino que una estimación para la diferencia de presión media entre dos superficie. En esta tesis también introducimos un nuevo enfoque inspirado en el WERP, que llamamos IMRP: en vez de multiplicar por la velocidad e integrar para obtener un balance de energía, multiplicamos por una función test auxiliar con el objetivo de obtener la presión relativa a través de un balance integral de momento. Dos versiones serán P-IMRP y B-IMRP.

En síntesis, proponemos una serie de modificaciones de los algoritmos que estiman el salto de presión que en general mejoran los métodos y se pueden resumir como:

- Integrar por partes para reducir el orden de derivación, disminuyendo la amplificación del ruido.
- Usar funciones auxiliares distintas a las medidas y libres de ruido, para reducir la varianza y el sesgo de los estimadores.
- Aproximar la velocidad en el tiempo $t = (n + \frac{1}{2})\tau$, donde τ es el paso de tiempo, con un esquema $\boldsymbol{u}^{n+\frac{1}{2}} = \frac{\boldsymbol{u}^{n+1}+\boldsymbol{u}^{n}}{2}$. Esto reduce la varianza de los estimadores.

Concluimos que los métodos más robustos son STEint B-IMRP.

ESTIMATION OF RELATIVE PRESSURE FROM VELOCITY MEASUREMENTS IN BLOOD FLOWS: STATE-OF-THE-ART AND NEW APPROACHES

Pressure gradients in stenotic blood vessels are an important clinical index for diagnosis of the severity of cardiovascular pathologies. While the clinical gold standard for its measurement is invasive catheterization (to measure pressure direcly introducing a catheter into blood vessels), Phase-Contrast MR-Imaging has emerged as a promising tool for enabling a non-invasive quantification of the relative pressures, by linking the (highly spatially resolved) velocity measurements with the relative pressure via the incompressible Navier–Stokes equations. This work's objective is to review, propose and compare different estimation methods for pressure difference in a coarctation using numerical simulations of blood.

In this work we first provide a review of current methods for relative pressure estimation, i.e. the PPE, STE and WERP. After proposing some improvements to these methods, we present a family of approaches that integrate measurements over a control volume in order to recover the relative pressure. We did a comparative study with existent and proposed methods using synthetic data in 2D with noise.

PPE resolves a Poisson equation for pressure p using blood flow velocity data: $\boldsymbol{\nabla} p = f(\boldsymbol{u})$. STE adds a difusion term to this problem, adding a divergence-free perturbation $\boldsymbol{w}$ that should be almost null. This is to solve a Stokes problem: $-\Delta \boldsymbol{w} + \boldsymbol{\nabla} p = f(\boldsymbol{u})$. Both aproaches give a pressure estimation over the whole domain. In this work we propose to integrate by parts the right hand side of STE, reducing derivation orders.

Alternatively, WERP takes a different aproach, where we only ask for the pressure difference between two surfaces based on an integral energy balance. This method only requires to compute integrals over the domain using measured velocity, largely reducing its computation time. However, we don't get a pressure estimation over the whole domain, but a pressure difference estimation between two spatial points. In this work we also introduce a new aproach inspired from WERP, which we called IMRP. Instead of multiplying by the flow velocity and integrating to obtain an energy balance, we multiply by a auxiliary test function in order to obtain the relative pressure from an integral momentum balance.

In this work we found a number of modifications for the pressure estimation algorithms which, generally, improves the methods and can be summarized as follows.

- Integrate by parts to reduce derivation orders and noise amplification.
- Use noise-free auxiliary functions, different from measurements, to reduce the estimator variance and bias.
- Approximate velocity in time $t = (n + \frac{1}{2})\tau$, where τ is the time step, with a scheme $\boldsymbol{u}^{n+\frac{1}{2}} = \frac{\boldsymbol{u}^{n+1}+\boldsymbol{u}^{n}}{2}$, this reduces estimator's variance.

We conclude that the most robust methods are those with the improvements proposed in this work, meaning: STE integrated by parts and IMRP using an auxiliary test function of a Brinkman problem.

Naturally, these conclusions must be also validated with tridimensional simulations, but this goes beyond the original objective of this work, which is a first step in that direction.

Contents

Chapter 1

Introduction

Aortic coarctation is a congenital disease consisting of a stenosis of the aorta near its arc (Figure 1.1). Pressure difference between before and after the stenosis is a standard clinical measurement that serves to asses the severity of the pathology. It may be performed several times during diagnosis and follow up [1], in order to determine the need of a surgical intervention and/or a more intensive follow up.

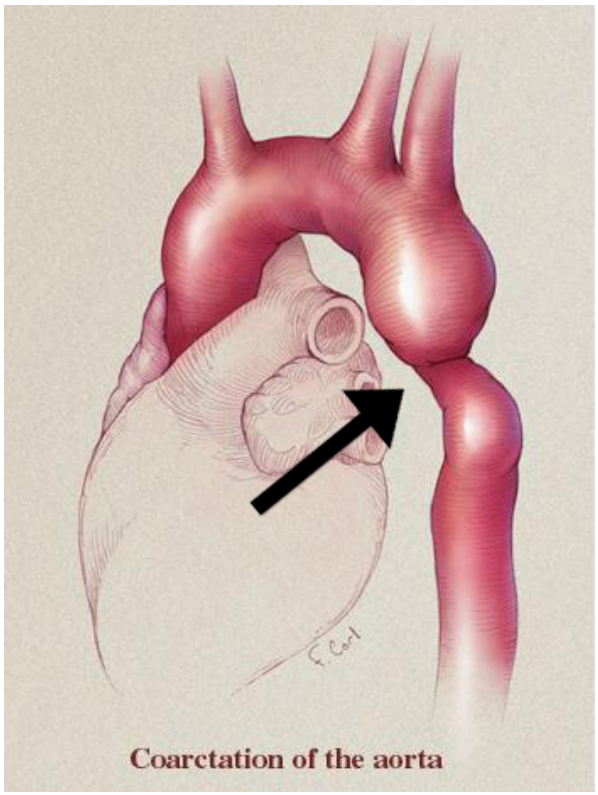

Figure 1.1: Aortic coarctation illustration from http://www.ctisus.com/

Moreover, peak instantaneous gradient also determines clinically the chance of re-coarctation after surgery [2, 3]. The most reliable procedure in clinical practice to obtain peak instantaneous pressure gradient involves the measurement of relative pressure invasively via catheteri-

zation, which has restricted indications and should be avoided unless non-invasive evaluations are inconclusive or discordant with clinical findings, given its potential risk [4].

Alternatively, Phase-Contrast Magnetic Resonance Imaging (PC-MRI) allows to obtain three-dimensional, time-resolved measurements of the velocity field, allowing visualization of complex blood flow patterns in large vessels and the heart [5]. Typical (recommended) PC-MRI spatial and temporal resolutions go from 1.5 to 3 mm^3 and $30 - 40$ ms, respectively [6]. Hence, it has been natural to postulate methods to compute the relative pressures using these measured velocities and the Navier–Stokes equations.

First in [7, 8], and revisited recently in the context of finite elements in [9], a relative pressure field was reconstructed by directly plugging the velocity measurements into a Navier–Stokes equation, and solving a Poisson equation for the pressure. This technique has the drawback that it requires second derivatives to evaluate the viscosity term. This approach is usually denoted by Pressure Poisson Estimator (PPE).

Recently in [10], the authors proposed to solve a Stokes problem, by adding a divergence-free vector to the Navier–Stokes residual, which results in a mixed problem for this vector and the pressure to be estimated. In the tests presented in [10], this technique gives better approximation results than the PPE.

Also very recently in [11], a new relation between relative pressure and velocity measurements was proposed by using the classical integral energy balance of the incompressible Navier–Stokes equations. This has the advantage that only few integrals have to be evaluated, making it computationally more efficient with respect to the PPE solution, and it only requires the first derivatives of the measured velocities. However, the authors indicated some potential drawbacks: (i) the measurement terms are squared, amplifying the noise, in particular for small in-/outflows, and (ii) it cannot be applied for simultaneous estimation of relative pressure in multiple outlet geometries.

Next we formulate an alternative integral approach of the momentum balance for estimating relative pressures. Instead of testing the Navier–Stokes equations by the measurements to obtain an energy-balance, we test it with an independent function, with the only requirements of zero divergence and zero normal component on the vessel walls, e.g. the solution of a simple static Stokes problem. We show that this overcomes the drawbacks of the energy-like approach of [11] in several numerical examples using synthetic data. Moreover, we prove that the method delivers an unbiased estimate with respect to the noise-free solution.

The rest of this paper is organized as follows. In Chapter 2 we set up the pressure estimation problem. In Chapter 3 we revisit the state-of-the-art methods mentioned above and propose some modifications that may improve their performance in Chapter 4. Then in Chapter 5, we derive the family of integral momentum pressure estimators. In Chapter 6 we test all methods using synthetic data, including sensitivity to noise, spatial and temporal subsampling. Finally in Chapter 7 we discuss the results, draw some conclusions and perspectives.

Chapter 2

The relative pressure estimation problem

Let us consider an incompressible, Newtonian fluid in a bounded domain $\Omega \subset \mathbb{R}^{\mathrm{d}}$, $\mathrm{d} = 2, 3$, modeled by the incompressible Navier–Stokes equations with the velocity $\boldsymbol{u}(t) : \Omega \to \mathbb{R}^{\mathrm{d}}$ and the pressure $p(t) : \Omega \to \mathbb{R}$, $t \in [0, T]$:

$$\begin{cases} \rho \partial_t \boldsymbol{u} + \rho(\boldsymbol{u} \cdot \boldsymbol{\nabla})\boldsymbol{u} - \mu \Delta \boldsymbol{u} + \boldsymbol{\nabla} p = \boldsymbol{0} \quad \text{in} \quad \Omega \times [0, T], \\ \boldsymbol{\nabla} \cdot \boldsymbol{u} = 0 \quad \text{in} \quad \Omega \times [0, T] \end{cases} \tag{2.1}$$

where ρ is the density and μ the dynamic viscosity. We also assume that the boundary of Ω given by $\partial\Omega := \Gamma = \Gamma_{\mathrm{i}} \cup \Gamma_o \cup \Gamma_w$, with $\Gamma_{\mathrm{i}} \cap \Gamma_o = \emptyset$. Γ_{i} is the inlet boundary (typically the one proximal to the heart), Γ_o the outlet (distal) boundary and Γ_w is the arterial wall boundary, as in Figure 2.1. The task of the relative pressure estimation is to compute:

$$\delta p = \frac{1}{|\Gamma_o|} \int_{\Gamma_o} p - \frac{1}{|\Gamma_{\mathrm{i}}|} \int_{\Gamma_{\mathrm{i}}} p \tag{2.2}$$

given (perturbed) measurements of $\boldsymbol{u}$ in Ω.

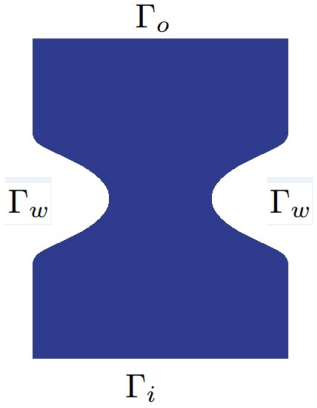

Figure 2.1: Aortic geometry with 60% coarctation. For a given geometry, we will call "coarctation percentage", $C\% = 100(1 - \frac{\text{minimum width}}{\text{maximum width}})\%$.

As is obtained in Phase-Contrast MRI, we will assume that the velocity measurements are available at h-spaced discrete points of the domain Ω, but we will be able to reconstruct them

everywhere by: (a) computing a mesh $\mathcal{T}_h$ of the domain Ω using the measurement locations, and then (b) interpolating the velocity components at every point in Ω using simple linear piecewise finite element basis functions. Additionally, we will asume that these space-discrete measurements will be available at N discrete measurement times $t^1, ..., t^N$ at a constant time interval τ. We will denote the measurements as $\boldsymbol{u}_m^1, ..., \boldsymbol{u}_m^N \in [\mathcal{P}_h^1]^{\mathrm{d}}$, with $\mathcal{P}_h^k$ the usual piecewise continuous k-th order polinomial finite element space.

Moreover, for further analysis we assume that the measurements include a random, additive perturbation with respect to the ground truth velocity, i.e. $\boldsymbol{u}_m^n = \boldsymbol{u}_h^n + \boldsymbol{\varepsilon}^n$, with $\boldsymbol{u}_h^n \in [\mathcal{P}_h^1]^{\mathrm{d}}$ a spatial subsampling of the true field $\boldsymbol{u}$ into $[\mathcal{P}_h^1]^{\mathrm{d}}$ at observation time t^n, and $\boldsymbol{\varepsilon}^n \in [\mathcal{P}_h^1]^{\mathrm{d}}$ a discrete noise field, with all degrees-of-freedom independently identically distributed (i.i.d.) following a normal distribution $\mathcal{N}(0, \sigma^2)$.

Chapter 3

State of the art of estimators

3.1 The Poisson Pressure Estimator (PPE)

The PPE, in the context of finite elements, is based on the assumption that the pressure gradient $\boldsymbol{\nabla} p$ satisfies a weak version of Equation (2.1). Hence, the estimated relative pressure at time $t^{n+1/2} := (t^n + t^{n+1})/2$ can be found as a solution of the following problem: Find $p_{ppe}^{n+1/2} \in \mathcal{P}_h^k$, $k \geq 1$, such that

$$\begin{aligned} \int_\Omega \boldsymbol{\nabla} p_{\text{ppe}}^{n+1/2} \boldsymbol{\nabla} q &= -\frac{\rho}{\tau} \int_\Omega (\boldsymbol{u}_m^{n+1} - \boldsymbol{u}_m^n) \cdot \boldsymbol{\nabla} q \\ &\quad -\rho \int_\Omega (\boldsymbol{u}_m^{n+1/2} \cdot \boldsymbol{\nabla} \boldsymbol{u}_m^{n+1/2}) \cdot \boldsymbol{\nabla} q \\ &\quad +\mu \int_\Omega \Delta \boldsymbol{u}_m^{n+1/2} \cdot \boldsymbol{\nabla} q \end{aligned} \tag{3.1}$$

for all $q \in \mathcal{P}_h^k$, and $p_{\text{ppe}} = q = 0$ on Γ_o.

Note that $\Delta \boldsymbol{u}_m$ is zero on each element of the mesh since $\boldsymbol{\nabla} \boldsymbol{u}_m$ is piecewise constant by element, but this is not true across the interfaces. Nevertheless, this term is usually neglected in blood flows by arguing that the viscous part of the pressure gradient is negligible [12].

Then, the pressure drop at time $t^{n+1/2}$ between the outlet and the inlet is evaluated with Equation (2.2) using $p_{\text{ppe}}^{n+1/2}$. Note that the midpoint time evaluation scheme allows a second order approximation with respect to time and to reduce the noise variance of the measurements $\boldsymbol{u}_m^{n+1/2}$ by a factor of 2 with respect to the original variance of the measurements $\boldsymbol{u}_m^n$. We obtain this property using that $\mathbb{E}(\boldsymbol{u}_m^n) = 0$, $\mathbb{V}(\boldsymbol{u}_m^n) = \sigma^2$, $\forall n$ as following:

$$\begin{aligned} \mathbb{V}(\boldsymbol{u}_m^{n+1/2}) &= \mathbb{E}\left((\boldsymbol{u}_m^{n+1/2})^2\right) - \left(\mathbb{E}(\boldsymbol{u}_m^{n+1/2})\right)^2 = \mathbb{E}\left(\left(\frac{\boldsymbol{u}_m^n + \boldsymbol{u}_m^{n+1}}{2}\right)^2\right) \\ &= \frac{1}{4}\left(\mathbb{E}\left((\boldsymbol{u}_m^n)^2\right) + \mathbb{E}\left(\left(\boldsymbol{u}_m^{n+1}\right)^2\right) + \mathbb{E}\left((\boldsymbol{u}_m^n) \cdot \left(\boldsymbol{u}_m^{n+1}\right)\right)\right) \\ &= \frac{1}{4}\left(\sigma^2 + \sigma^2 + 0\right) = \frac{\sigma^2}{2} \end{aligned}$$

This approach will be used for all the methods studied throughout the manuscript.

3.2 The Stokes estimator (STE)

The STE formulated in [10] consists in perturbing the Navier–Stokes equation with the Laplacian of an auxiliar divergence-free velocity field $\boldsymbol{w}$. This leads to a mixed problem for the pressure, in terms of the measured velocity, instead of a Poisson problem as in the PPE.

The STE is formulated as follows for the time step $t^{n+1/2}$. Find $\boldsymbol{w} \in [\mathcal{P}_h^1 + \text{bubble}]^{\text{d}}$ and $p_{ste}^{n+1/2} \in \mathcal{P}_h^1$, such that

$$\begin{aligned} \int_\Omega \boldsymbol{\nabla w} : \boldsymbol{\nabla \hat{w}} - \int_\Omega p_{ste}^{n+1/2} (\boldsymbol{\nabla} \cdot \hat{\boldsymbol{w}}) + \int_\Omega (\boldsymbol{\nabla} \cdot \boldsymbol{w}) q \;\; = \;\; & -\frac{\rho}{\tau} \int_\Omega (\boldsymbol{u}_m^{n+1} - \boldsymbol{u}_m^n) \cdot \hat{\boldsymbol{w}} \\ & -\rho \int_\Omega (\boldsymbol{u}_m^{n+1/2} \cdot \boldsymbol{\nabla u}_m^{n+1/2}) \cdot \hat{\boldsymbol{w}} \\ & +\mu \int_\Omega \Delta \boldsymbol{u}_m^{n+1/2} \cdot \hat{\boldsymbol{w}} \end{aligned} \tag{3.2}$$

for all $\hat{\boldsymbol{w}} \in [\mathcal{P}_h^1 + \text{bubble}]^{\text{d}}$ and $q \in \mathcal{P}_h^1$, with $\boldsymbol{w} = \hat{\boldsymbol{w}} = \boldsymbol{0}$ on Γ. Then, the pressure drop at time $t^{n+1/2}$ between the outlet and the inlet is evaluated with Formula (2.2) using $p_{\text{ste}}^{n+1/2}$.

Let b be a bubble base function, T a finite element and c_T the centroid of that element. Then $b(c_T) = 1$ and $b(x) = 0,\ \forall x \in \partial T$. We add a bubble test function to $[\mathcal{P}_h^1]^{\text{d}}$ to obtain an inf-sup stable mixed formulation, thus, obtaining a well posed problem [13].

Note that, as for the PPE, the viscous term of the right-hand-side of (3.2) is not identically zero, nevertheless, it is usually neglected in blood flows by arguing that the viscous part of the pressure gradient is negligible [12].

3.3 The work-energy relative pressure estimator (WERP)

The starting point of the formulation of the WERP method introduced in [11] is the classical energy relation of an incompressible Newtonian fluid, which can be obtained either by writing the conservation law for the energy density $\rho \boldsymbol{u}^2/2$ directly or multiplying (2.1) by $\boldsymbol{u}$ and integrating over Ω. This relation reads

$$\frac{\rho}{2} \int_\Omega \partial_t (|\boldsymbol{u}|^2) + \frac{\rho}{2} \int_\Gamma (\boldsymbol{u} \cdot \boldsymbol{n}) |\boldsymbol{u}|^2 + \mu \int_\Omega |\boldsymbol{\nabla u}|^2 + \int_\Gamma p\, (\boldsymbol{u} \cdot \boldsymbol{n}) - \mu \int_\Gamma (\boldsymbol{\nabla u} \cdot \boldsymbol{n}) \cdot \boldsymbol{u} = 0\ . \tag{3.3}$$

with $|\cdot|$ denoting the Euclidian norm.

The WERP is then formulated by assuming that: (i) the measurements $\boldsymbol{u}_m^n$ satisfy relation (3.3), (ii) $\boldsymbol{u}_m^n \cdot \boldsymbol{n} \approx 0$ on Γ_w (i.e. the vessel walls nearly don't move), (iii) the viscous forces on

Γ are negligible, (iv) and the pressure is nearly constant on Γ_{i} and Γ_o. Doing so, the WERP pressure estimator at time $t^{n+1/2}$ is written as:

$$\delta p_{werp}^{n+1/2}(\boldsymbol{u}_m^{n,n+1}) = -\frac{1}{\Lambda(\boldsymbol{u}_m^{n+1/2})}\left(E_{kin}(\boldsymbol{u}_m^{n+1}) - E_{kin}(\boldsymbol{u}_m^{n}) + E_{conv}(\boldsymbol{u}_m^{n+1/2}) + E_{visc}(\boldsymbol{u}_m^{n+1/2})\right) \tag{3.4}$$

with

$$E_{kin}(\boldsymbol{w}) = \frac{\rho}{2\tau}\int_\Omega |\boldsymbol{w}|^2 \tag{3.5}$$

$$E_{conv}(\boldsymbol{w}) = \frac{\rho}{2}\int_{\Gamma_{\mathrm{i}}\cup\Gamma_o} (\boldsymbol{w}\cdot\boldsymbol{n})|\boldsymbol{w}|^2 \tag{3.6}$$

$$E_{visc}(\boldsymbol{w}) = \mu\int_\Omega |\boldsymbol{\nabla w}|^2 - \mu\int_\Gamma (\boldsymbol{\nabla w}\cdot\boldsymbol{n})\cdot\boldsymbol{w} \tag{3.7}$$

$$\Lambda(\boldsymbol{w}) = \int_{\Gamma_{\mathrm{i}}} \boldsymbol{w}\cdot\boldsymbol{n}. \tag{3.8}$$

As it is well known from numerical analysis, the use of the mid-point scheme in (3.4) does not induce any perturbation compared with the time-continuous energy relation (3.3), independently on the time step τ.

We can see that this formulation may be unstable at small in-/outflows due to the division by $\Lambda(\boldsymbol{u}_m^{n+1/2})$. In other words, when the inflow is small, perturbations (e.g. due to the noise) can induce large errors in $\Lambda(\boldsymbol{u}_m^{n+1/2})$ leading to an unphysical amplification of the estimated relative pressure. Another relevant issue is that the WERP induces systematic shifts in the pressure curve in the presence of noise, as we will see in the next section. Moreover, the WERP can only by construction estimate relative pressure in geometries with only one inflow and one outflow, due to the assumption $\boldsymbol{u}_m^n\cdot\boldsymbol{n}\approx 0$

Chapter 4

Modified estimation methods

In this section, we present modifications of the STE and WERP methods, and we will see later in the numerical examples that they can lead to improvements in the estimation results.

4.1 The integrated STE (STEint)

We propose to modify the STE method originally proposed in [10] and formulated in Equation (3.2) by taking advantage of the regularity of the auxiliar velocity field and integrating by parts the convective and viscous term.

The STEint is formulated as follows for the time step $t^{n+1/2}$. Find $\boldsymbol{w} \in [\mathcal{P}_h^1 + \text{bubble}]^{\text{d}}$ and $p_{st\text{ei}}^{n+1/2} \in \mathcal{P}_h^1$, such that

$$\begin{aligned}\int_\Omega \boldsymbol{\nabla w} : \boldsymbol{\nabla \hat{w}} - \int_\Omega p_{st\text{ei}}^{n+1/2}(\boldsymbol{\nabla}\cdot\boldsymbol{\hat{w}}) + \int_\Omega (\boldsymbol{\nabla}\cdot\boldsymbol{w})q \;\; = \;\; & -\frac{\rho}{\tau}\int_\Omega (\boldsymbol{u}_m^{n+1} - \boldsymbol{u}_m^n)\cdot\boldsymbol{\hat{w}} \\ & +\rho\int_\Omega (\boldsymbol{u}_m^{n+1/2}\cdot\boldsymbol{\nabla\hat{w}})\cdot\boldsymbol{u}_m^{n+1/2} \\ & -\mu\int_\Omega \boldsymbol{\nabla u}_m^{n+1/2} : \boldsymbol{\nabla\hat{w}} \qquad (4.1)\end{aligned}$$

for all $\boldsymbol{\hat{w}} \in [\mathcal{P}_h^1 + \text{bubble}]^{\text{d}}$ and $q \in \mathcal{P}_h^1$, with $\boldsymbol{w} = \boldsymbol{\hat{w}} = \boldsymbol{0}$ on Γ.

Note that the boundary terms of the integration by parts do not appear since $\boldsymbol{\hat{w}} = \boldsymbol{0}$. We point out that this integration by parts is not obvious for the PPE method due to the lack of enough regularity of $\boldsymbol{\nabla} q$ in Equation (3.1) when standard finite element spaces are used (like $\mathcal{P}_h^k$).

Then, the pressure drop at time $t^{n+1/2}$ between the outlet and the inlet is evaluated with Formula (2.2) using $p_{\text{stei}}^{n+1/2}$.

4.2 The Darcy (DAE) and the integrated Darcy (DAEint) estimators

Note that, a similar alternative for the STE would be to use a Darcy formulation for $\boldsymbol{w}$ instead of Stokes:

Let $\mathcal{RT}_h^k$ be the usual Raviart-Thomas finite element space of degree k. Then, find $\boldsymbol{w} \in \mathcal{RT}_h^k$ and $p_{\text{dae}}^{n+1/2} \in \mathcal{P}_h^k$, $k \geq 0$, such that

$$\begin{aligned}\int_\Omega \boldsymbol{w}\cdot\hat{\boldsymbol{w}} - \int_\Omega p_{\text{dae}}^{n+1/2}(\boldsymbol{\nabla}\cdot\hat{\boldsymbol{w}}) + \int_\Omega (\boldsymbol{\nabla}\cdot\boldsymbol{w})q \;&=\; -\frac{\rho}{\tau}\int_\Omega (\boldsymbol{u}_m^{n+1}-\boldsymbol{u}_m^n)\cdot\hat{\boldsymbol{w}} \\ &\quad -\rho\int_\Omega (\boldsymbol{u}_m^{n+1/2}\cdot\boldsymbol{\nabla}\boldsymbol{u}_m^{n+1/2})\cdot\hat{\boldsymbol{w}} \\ &\quad +\mu\int_\Omega \Delta\boldsymbol{u}_m^{n+1/2}\cdot\hat{\boldsymbol{w}} \end{aligned} \tag{4.2}$$

for all $\hat{\boldsymbol{w}} \in \mathcal{RT}_h^k$ and $q \in \mathcal{P}_h^k$, with $\boldsymbol{w}\cdot\boldsymbol{n} = \hat{\boldsymbol{w}}\cdot\boldsymbol{n} = 0$ on Γ. This approach has not been yet reported, to the authors best knowledge.

Analogously to STEint, we can also integrate by parts the right-hand-side of DAE, and formulate the following new estimator problem that we will call DAEint: Find $\boldsymbol{w} \in \mathcal{RT}_h^k$ and $p_{\text{daei}}^{n+1/2} \in \mathcal{P}_h^k$, $k \geq 0$, such that

$$\begin{aligned}\int_\Omega \boldsymbol{w}\cdot\hat{\boldsymbol{w}} - \int_\Omega p_{\text{daei}}^{n+1/2}(\boldsymbol{\nabla}\cdot\hat{\boldsymbol{w}}) + \int_\Omega (\boldsymbol{\nabla}\cdot\boldsymbol{w})q \;&=\; -\frac{\rho}{\tau}\int_\Omega (\boldsymbol{u}_m^{n+1}-\boldsymbol{u}_m^n)\cdot\hat{\boldsymbol{w}} \\ &\quad +\rho\int_\Omega (\boldsymbol{u}_m^{n+1/2}\cdot\boldsymbol{\nabla}\hat{\boldsymbol{w}})\cdot\boldsymbol{u}_m^{n+1/2} \\ &\quad -\rho\int_\Gamma (\boldsymbol{u}_m^{n+1/2}\cdot\boldsymbol{n})(\boldsymbol{u}_m^{n+1/2}\cdot\hat{\boldsymbol{w}}) \\ &\quad -\mu\int_\Omega \boldsymbol{\nabla}\boldsymbol{u}_m^{n+1/2} : \boldsymbol{\nabla}\hat{\boldsymbol{w}} \\ &\quad +\mu\int_\Gamma (\boldsymbol{\nabla}\boldsymbol{u}_m^{n+1/2}\cdot\boldsymbol{n})\cdot\hat{\boldsymbol{w}} \end{aligned} \tag{4.3}$$

for all $\hat{\boldsymbol{w}} \in \mathcal{RT}_h^k$ and $q \in \mathcal{P}_h^k$, with $\boldsymbol{w}\cdot\boldsymbol{n} = \hat{\boldsymbol{w}}\cdot\boldsymbol{n} = 0$ on Γ.

4.3 The corrected WERP (c-WERP)

In order to propose a correction for the WERP, we first need to analyze its bias. We notice that this was not done in the original article [11].

Consider $\boldsymbol{M}_\Omega$ and $\boldsymbol{K}_\Omega$ the classical mass and stiffness finite element matrices for the Stokes problem in Ω, respectively. Then, let us point out that the following identities hold:

$$\mathbb{E}\left(\frac{\rho}{2}\int_\Omega \boldsymbol{\varepsilon}^n\cdot\boldsymbol{w}\right) = 0\ ,\ \mathbb{E}\left(\int_\Omega \boldsymbol{\nabla}\boldsymbol{w} : \boldsymbol{\nabla}\boldsymbol{\varepsilon}^n\right) = 0 \tag{4.4}$$

for any deterministic function $\boldsymbol{w}$, and

$$\mathbb{E}\left(\frac{\rho}{2\tau}\int_\Omega |\boldsymbol{\varepsilon}^n|^2\right) = \sigma^2\,\mathrm{tr}(\boldsymbol{M}_\Omega),\ \mathbb{E}\left(\mu\int_\Omega |\boldsymbol{\nabla}\boldsymbol{\varepsilon}^{n+1/2}|^2\right) = \frac{\sigma^2}{2}\,\mathrm{tr}(\boldsymbol{K}_\Omega)\ . \tag{4.5}$$

Note that for the last term, we use the fact that the variance of the nodal values of $\boldsymbol{\varepsilon}^{n+1/2}$ are $\sigma^2/2$.

The goal is now to compute $\mathbb{E}(\delta p_{werp}^{n+1/2}(\boldsymbol{u}_m^{n,n+1}))$. In order to perform such an analysis, we include an additional assumption that $\Lambda(\boldsymbol{u}_m^{n+1/2}) \approx \Lambda(\boldsymbol{u}_h^{n+1/2})$, which is reasonable if we are interested in estimating the peak relative pressure, which typically is simultaneous to the peak flow where the signal-to-noise ratio is best.

We proceed therefore as follows:

$$\mathbb{E}(\delta p_{werp}^{n+1/2}(\boldsymbol{u}_m^{n,n+1})) \approx -\frac{1}{\Lambda(\boldsymbol{u}_m^{n+1/2})}\mathbb{E}\left(E_{kin}(\boldsymbol{u}_m^{n+1}) - E_{kin}(\boldsymbol{u}_m^n) + E_{conv}(\boldsymbol{u}_m^{n+1/2}) + E_{visc}(\boldsymbol{u}_m^{n+1/2})\right)\ .$$

We now compute separately each term. First the kinetic part

$$\begin{aligned}
\mathbb{E}\left(E_{kin}(\boldsymbol{u}_m^n)\right) &= \mathbb{E}\left(\frac{\rho}{2\tau}\int_\Omega |\boldsymbol{u}_h^n + \boldsymbol{\varepsilon}^n|^2\right)\\
&= \frac{\rho}{2\tau}\int_\Omega \mathbb{E}\left(|\boldsymbol{u}_h^n|^2 + 2\boldsymbol{u}_h^n\cdot\boldsymbol{\varepsilon}^n + |\boldsymbol{\varepsilon}^n|^2\right)\\
&= E_{kin}(\boldsymbol{u}_h^n) + \sigma^2\,\mathrm{tr}(\boldsymbol{M}_\Omega)\ .
\end{aligned}$$

Then, the convective part

$$\begin{aligned}
\mathbb{E}\left(E_{conv}(\boldsymbol{u}_m^n)\right) &= \frac{\rho}{2}\int_{\Gamma_\mathrm{i}\cup\Gamma_o} \mathbb{E}\left(((\boldsymbol{u}_h^n + \boldsymbol{\varepsilon}^n)\cdot\boldsymbol{n})|\boldsymbol{u}_h^n + \boldsymbol{\varepsilon}^n|^2\right)\\
&= \frac{\rho}{2}\int_{\Gamma_\mathrm{i}\cup\Gamma_o} \mathbb{E}\big((\boldsymbol{u}_h^n\cdot\boldsymbol{n})\left\{|\boldsymbol{u}_h^n|^2 + 2\boldsymbol{u}_h^n\cdot\boldsymbol{\varepsilon}^n + |\boldsymbol{\varepsilon}^n|^2\right\}\\
&\qquad +(\boldsymbol{\varepsilon}^n\cdot\boldsymbol{n})\left\{|\boldsymbol{u}_h^n|^2 + 2\boldsymbol{u}_h^n\cdot\boldsymbol{\varepsilon}^n + |\boldsymbol{\varepsilon}^n|^2\right\}\big)\\
&= E_{conv}(\boldsymbol{u}_h^n) + \frac{\rho}{2}\int_{\Gamma_\mathrm{i}\cup\Gamma_o} \mathbb{E}\left((\boldsymbol{u}_h^n\cdot\boldsymbol{n})|\boldsymbol{\varepsilon}^n|^2 + 2(\boldsymbol{\varepsilon}^n\cdot\boldsymbol{n})(\boldsymbol{u}_h^n\cdot\boldsymbol{\varepsilon}^n)\right)\\
&= E_{conv}(\boldsymbol{u}_h^n) + B_{conv}(\boldsymbol{u}_h^n, \sigma^2)\ .
\end{aligned}$$

where it can be easily shown that the very last (cubic) term in the second row vanishes due to the standard result that the cube of a normal variable has also zero expected value. And at last, the viscous part

$$\begin{aligned}
\mathbb{E}\left(E_{visc}(\boldsymbol{u}_m^{n+1/2})\right) &= E_{visc}(\boldsymbol{u}_h^{n+1/2}) + \mu\int_\Omega 2\boldsymbol{\nabla}\boldsymbol{u}_h^{n+1/2} : \boldsymbol{\nabla}\boldsymbol{\varepsilon}^{n+1/2} + |\boldsymbol{\nabla}\boldsymbol{\varepsilon}^{n+1/2}|^2\\
&= E_{visc}(\boldsymbol{u}_h^{n+1/2}) + \frac{\sigma^2}{2}\,\mathrm{tr}(\boldsymbol{K}_\Omega)\ .
\end{aligned}$$

Now, summing all the terms we obtain the following expression for the bias of the WERP estimator

$$\mathbb{E}(\delta p_{werp}^{n+1/2}(\boldsymbol{u}_m^{n,n+1})) - \delta p_{werp}^{n+1/2}(\boldsymbol{u}_h^{n,n+1}) \approx -\frac{1}{\Lambda(\boldsymbol{u}_m^{n+1/2})}\left(B_{conv}(\boldsymbol{u}_h^{n+1/2}, \sigma^2) + \frac{\sigma^2}{2}\operatorname{tr}(\boldsymbol{K}_\Omega)\right) . \tag{4.6}$$

Note that $B_{conv}(\boldsymbol{u}_h^n, \boldsymbol{\varepsilon}^n)$ depends on both real (unknown) spatially subsampled velocity $\boldsymbol{u}_h^{n+1/2}$ and noise variance σ^2, while the second term of the bias depends on σ^2 and the geometry Ω only.

From (4.6), in the case when the noise statistics are known, we propose a corrected version of the WERP, what we will call c-WERP estimator

$$\delta p_{c-werp}^{n+1/2}(\boldsymbol{u}_m^{n,n+1})) = \delta p_{werp}^{n+1/2}(\boldsymbol{u}_m^{n,n+1})) + \frac{1}{\Lambda(\boldsymbol{u}_m^{n+1/2})}\frac{\sigma^2}{2}\operatorname{tr}(\boldsymbol{K}_\Omega). \tag{4.7}$$

Chapter 5

Integral momentum relative pressure estimators

In this section we derive a new formulation for the integral relative pressure estimator based on a general class of test functions, and we will analyze it in terms of its bias.

5.1 Formulation

Assume that we have computed a discrete function $\boldsymbol{v}$ (in some finite element space in $\mathcal{T}_h$), satisfying

$$\boldsymbol{\nabla} \cdot \boldsymbol{v} \approx 0 \ , \ \boldsymbol{v} \cdot \boldsymbol{n} = 0 \text{ on } \Gamma_w \tag{5.1}$$

If we multiply Equation (2.1) by $\boldsymbol{v}$ and we integrate over Ω

$$\underbrace{\rho \int_\Omega \partial_t \boldsymbol{u} \cdot \boldsymbol{v}}_{I_{kin}(\partial_t \boldsymbol{u})} + \underbrace{\rho \int_\Omega (\boldsymbol{u} \cdot \boldsymbol{\nabla} \boldsymbol{u}) \cdot \boldsymbol{v}}_{I_{conv}(\boldsymbol{u})} + \underbrace{\int_\Omega \boldsymbol{\nabla} p \cdot \boldsymbol{v}}_{I_{pres}} \underbrace{-\mu \int_\Omega \Delta \boldsymbol{u} \cdot \boldsymbol{v}}_{I_{visc}(\boldsymbol{u})} = 0 \ . \tag{5.2}$$

we obtain for each of the terms

$$I_{conv}(\boldsymbol{u}) = -\rho \int_\Omega (\boldsymbol{u} \cdot \boldsymbol{\nabla} \boldsymbol{v}) \cdot \boldsymbol{u} + \rho \int_\Gamma (\boldsymbol{u} \cdot \boldsymbol{n})(\boldsymbol{u} \cdot \boldsymbol{v}) \tag{5.3}$$

$$I_{pres} = -\int_\Omega p(\boldsymbol{\nabla} \cdot \boldsymbol{v}) + \int_\Gamma p\,(\boldsymbol{v} \cdot \boldsymbol{n}) = \int_{\Gamma_i \cup \Gamma_o} p\,(\boldsymbol{v} \cdot \boldsymbol{n}) \tag{5.4}$$

$$I_{visc}(\boldsymbol{u}) = \mu \int_\Omega \boldsymbol{\nabla} \boldsymbol{u} : \boldsymbol{\nabla} \boldsymbol{v} - \mu \int_\Gamma (\boldsymbol{\nabla} \boldsymbol{u} \cdot \boldsymbol{n}) \cdot \boldsymbol{v} \tag{5.5}$$

using standard integration by parts. We will only detail $I_{conv}(\boldsymbol{u})$ and we will work in $\mathbb{R}^2$, but it is similar for $\mathbb{R}^3$.

Let $\boldsymbol{\nabla u} = \begin{bmatrix} \partial_x \boldsymbol{u}_x & \partial_x \boldsymbol{u}_y \\ \partial_y \boldsymbol{u}_x & \partial_y \boldsymbol{u}_y \end{bmatrix}$ and where $(\boldsymbol{u} \cdot \boldsymbol{\nabla u})$ is a notation for $(\boldsymbol{\nabla u}^T \cdot \boldsymbol{u})$ with $\boldsymbol{u}$ a column vector.

$$\begin{aligned}
(\boldsymbol{u} \cdot \boldsymbol{\nabla u}) \cdot \boldsymbol{v} &= \begin{bmatrix} \boldsymbol{u}_x \partial_x \boldsymbol{u}_x + \boldsymbol{u}_y \partial_y \boldsymbol{u}_x & \boldsymbol{u}_x \partial_x \boldsymbol{u}_y + \boldsymbol{u}_y \partial_y \boldsymbol{u}_y \end{bmatrix} \cdot \begin{bmatrix} \boldsymbol{v}_x \\ \boldsymbol{v}_y \end{bmatrix} \\
&= \boldsymbol{u}_x \partial_x \boldsymbol{u}_x \boldsymbol{v}_x + \boldsymbol{u}_y \partial_y \boldsymbol{u}_x \boldsymbol{v}_x + \boldsymbol{u}_x \partial_x \boldsymbol{u}_y \boldsymbol{v}_y + \boldsymbol{u}_y \partial_y \boldsymbol{u}_y \boldsymbol{v}_y \\
&= \boldsymbol{u}_x (\partial_x \boldsymbol{u}_x \boldsymbol{v}_x + \partial_x \boldsymbol{u}_y \boldsymbol{v}_y) + \boldsymbol{u}_y (\partial_y \boldsymbol{u}_x \boldsymbol{v}_x + \partial_y \boldsymbol{u}_y \boldsymbol{v}_y) \\
&= \boldsymbol{u}_x \left((\partial_x (\boldsymbol{u}_x \boldsymbol{v}_x) - \boldsymbol{u}_x \partial_x \boldsymbol{v}_x) + (\partial_x (\boldsymbol{u}_y \boldsymbol{v}_y) - \boldsymbol{u}_y \partial_x \boldsymbol{v}_y) \right) \\
&\quad + \boldsymbol{u}_y \left((\partial_y (\boldsymbol{u}_x \boldsymbol{v}_x) - \boldsymbol{u}_x \partial_y \boldsymbol{v}_x) + (\partial_y (\boldsymbol{u}_y \boldsymbol{v}_y) - \boldsymbol{u}_y \partial_y \boldsymbol{v}_y) \right) \\
&= \boldsymbol{u}_x \partial_x (\boldsymbol{u}_x \boldsymbol{v}_x + \boldsymbol{u}_y \boldsymbol{v}_y) + \boldsymbol{u}_y \partial_y (\boldsymbol{u}_x \boldsymbol{v}_x + \boldsymbol{u}_y \boldsymbol{v}_y) \\
&\quad - \boldsymbol{u}_x^2 \partial_x \boldsymbol{v}_x - \boldsymbol{u}_x \boldsymbol{u}_y \partial_x \boldsymbol{v}_y - \boldsymbol{u}_y \boldsymbol{u}_x \partial_y \boldsymbol{v}_x - \boldsymbol{u}_y^2 \partial_y \boldsymbol{v}_y \\
&= \boldsymbol{u}_x \partial_x (\boldsymbol{u} \cdot \boldsymbol{v}) + \boldsymbol{u}_y \partial_y (\boldsymbol{u} \cdot \boldsymbol{v}) - \alpha_{\boldsymbol{v}} \\
&= \boldsymbol{u} \cdot (\boldsymbol{\nabla} (\boldsymbol{u} \cdot \boldsymbol{v})) - \alpha_{\boldsymbol{v}}
\end{aligned}$$

With $\alpha_{\boldsymbol{v}} = -\boldsymbol{u}_x^2 \partial_x \boldsymbol{v}_x - \boldsymbol{u}_x \boldsymbol{u}_y \partial_x \boldsymbol{v}_y - \boldsymbol{u}_y \boldsymbol{u}_x \partial_y \boldsymbol{v}_x - \boldsymbol{u}_y^2 \partial_y \boldsymbol{v}_y$

So we have,

$$\begin{aligned}
I_{conv}(\boldsymbol{u}) &= \rho \int_\Omega \boldsymbol{u} \cdot (\boldsymbol{\nabla} (\boldsymbol{u} \cdot \boldsymbol{v})) - \rho \int_\Omega \alpha_{\boldsymbol{v}} \\
&= -\rho \int_\Omega (\boldsymbol{\nabla} \cdot \boldsymbol{u})(\boldsymbol{u} \cdot \boldsymbol{v}) + \rho \int_\Gamma (\boldsymbol{u} \cdot n)(\boldsymbol{u} \cdot \boldsymbol{v}) - \rho \int_\Omega \alpha_{\boldsymbol{v}} \\
&= \rho \int_\Gamma (\boldsymbol{u} \cdot n)(\boldsymbol{u} \cdot \boldsymbol{v}) - \rho \int_\Omega \alpha_{\boldsymbol{v}}
\end{aligned}$$

assuming that $\boldsymbol{\nabla} \cdot \boldsymbol{u} = 0$.

Now, lets see that we can write $\alpha_{\boldsymbol{v}}$ as $(\boldsymbol{u} \cdot \boldsymbol{\nabla v}) \cdot \boldsymbol{u}$.

$$\begin{aligned}
(\boldsymbol{u} \cdot \boldsymbol{\nabla v}) \cdot \boldsymbol{u} &= \left(\begin{bmatrix} \boldsymbol{u}_x & \boldsymbol{u}_y \cdot \end{bmatrix} \begin{bmatrix} \partial_x \boldsymbol{v}_x & \partial_x \boldsymbol{v}_y \\ \partial_y \boldsymbol{v}_x & \partial_y \boldsymbol{v}_y \end{bmatrix} \right) \cdot \begin{bmatrix} \boldsymbol{u}_x \\ \boldsymbol{u}_y \end{bmatrix} \\
&= \begin{bmatrix} \boldsymbol{u}_x \partial_x \boldsymbol{v}_x + \boldsymbol{u}_y \partial_y \boldsymbol{v}_x & \boldsymbol{u}_x \partial_x \boldsymbol{v}_y + \boldsymbol{u}_y \partial_y \boldsymbol{v}_y \cdot \end{bmatrix} \cdot \begin{bmatrix} \boldsymbol{u}_x \\ \boldsymbol{u}_y \end{bmatrix} \\
&= \boldsymbol{u}_x^2 \partial_x \boldsymbol{v}_x + \boldsymbol{u}_x \boldsymbol{u}_y \partial_y \boldsymbol{v}_x + \boldsymbol{u}_y \boldsymbol{u}_x \partial_x \boldsymbol{v}_y + \boldsymbol{u}_y^2 \partial_y \boldsymbol{v}_y \\
&= \alpha_{\boldsymbol{v}} \ .
\end{aligned}$$

Therefore, we conclude

$$I_{conv}(\boldsymbol{u}) = -\rho \int_\Omega (\boldsymbol{u} \cdot \boldsymbol{\nabla v}) \cdot \boldsymbol{u} + \rho \int_\Gamma (\boldsymbol{u} \cdot n)(\boldsymbol{u} \cdot \boldsymbol{v}) \ .$$

The integral momentum relative pressure estimator (IMRP) is then formulated by assuming that: (i) the measurements $\boldsymbol{u}_m^n$ satisfy relation (5.2), (ii) the pressure is nearly constant

on Γ_{i} and Γ_o. Doing so, the IMRP estimator at time $t^{n+1/2}$ is formulated as:

$$\delta p_{\mathrm{imrp}}^{n+1/2}(\boldsymbol{u}_m^{n,n+1}) = -\frac{1}{\Lambda(\boldsymbol{v})}\left(I_{kin}(\frac{\boldsymbol{u}_m^{n+1}-\boldsymbol{u}_m^{n}}{\tau}) + I_{conv}(\boldsymbol{u}_m^{n+1/2}) + I_{visc}(\boldsymbol{u}_m^{n+1/2})\right) \ . \tag{5.6}$$

Note that the requirements on the test function in (5.1) serve only so that the pressure field vanishes (up to the relative pressure) in (5.4).

Notice also that the integral of the measurements are multiplied by $1/\Lambda(\boldsymbol{v})$, which is independent of the measurements. This is an advantage compared to the WERP for the potential spurious amplifications for low flows. Another advantage will be clear after the bias analysis. We also point out that we did not make any assumption on the velocity measurements on the boundary Γ_w, as it was done for the WERP. Hence it is potentially better at capturing the pressure gradient changes due to the wall deformation.

5.2 Choice of the test function

We propose the test function $\boldsymbol{v}$ as the solution of the following problems

P-IMRP: Weighting with a Poiseuille flow, i.e. a Stokes flow solution with unitary Neumann load on Γ_{i}: Find $\boldsymbol{v} \in [\mathcal{P}_h^1 + \mathrm{bubble}]^{\mathrm{d}}$ and $z \in \mathcal{P}_h^1$,

$$\int_\Omega \boldsymbol{\nabla v} : \boldsymbol{\nabla \psi} + \int_\Omega z \boldsymbol{\nabla} \cdot \boldsymbol{\psi} + \int_\Omega q \boldsymbol{\nabla} \cdot \boldsymbol{v} + \int_{\Gamma_{\mathrm{i}}} \boldsymbol{\psi} \cdot \boldsymbol{n} = 0 \ , \tag{5.7}$$

for all $\boldsymbol{\psi} \in [\mathcal{P}_h^1 + \mathrm{bubble}]^{\mathrm{d}}$ and $q \in \mathcal{P}_h^1$, and with $\boldsymbol{v} = \boldsymbol{\psi} = \boldsymbol{0}$ on Γ_w.

B-IMRP: Weighting with a Brinkman flow solution with Dirichlet boundary conditions for $\boldsymbol{v} \cdot \boldsymbol{n}$. Find $\boldsymbol{v} \in [\mathcal{P}_h^1 + \mathrm{bubble}]^{\mathrm{d}}$ and $z \in \mathcal{P}_h^1$

$$\int_\Omega \boldsymbol{v} \cdot \boldsymbol{\psi} + \nu \int_\Omega \boldsymbol{\nabla v} : \boldsymbol{\nabla \psi} - \nu \int_\Gamma \boldsymbol{\psi} \cdot (\boldsymbol{n}^\intercal \boldsymbol{\nabla v}) + \int_\Omega z \boldsymbol{\nabla} \cdot \boldsymbol{\psi} + \int_\Omega q \boldsymbol{\nabla} \cdot \boldsymbol{v} + \gamma \int_{\Gamma_w} (\boldsymbol{v} \cdot \boldsymbol{n})(\boldsymbol{\psi} \cdot \boldsymbol{n}) = 0 \ . \tag{5.8}$$

for all $\boldsymbol{\psi} \in [\mathcal{P}_h^1 + \mathrm{bubble}]^{\mathrm{d}}$ and $q \in \mathcal{P}_h^1$, and with $\boldsymbol{v}$ satisfying the Dirichlet boundary conditions $\boldsymbol{v} \cdot \boldsymbol{n} = -1$ on Γ_{i}, $\boldsymbol{v} \cdot \boldsymbol{n} = (|\Gamma_{\mathrm{i}}|/|\Gamma_o|)$ on Γ_o. The scalar $\gamma > 0$ is only one large penalization parameter.

The following remarks are in order:

Remark 1. *It is not necessary to introduce any coefficient in the viscous term in 5.7 since the IMRP estimator is insensitive to any constant scaling of the velocity field, see Equation* (5.6)*. Concerning the B-IMRP, note that the shape of the velocity field (and not only the scaling) changes with the viscosity* ν*.*

Remark 2. *A further option would be to include convective terms for* $\boldsymbol{v}$*. However, in our numerical experiments, this gave worse approximation results of the IMRP than testing with pure Stokes and Brinkman solutions. Therefore, we do not present any results for the sake of the manuscript's conciseness.*

Remark 3. *The finite element spaces of the weighting functions are defined in terms of standard mini elements. These are, however, not the only options. Alternatively, Taylor–Hood or Scott–Vogelius (strongly zero-divergence) [14] mixed elements can be used. However, the final relative pressure estimation does not considerably depend on the the order of the finite element space used for the test function. Differences between the different spaces can only be appreciated for coarse mesh spacing of the measurements, i.e. larger than* 3 *mm.*

5.3 Analysis of the IMRP estimator bias

As proceeded for the WERP, the aim is to compute

$$\mathbb{E}(\delta p_{\text{imrp}}^{n+1/2}(\boldsymbol{u}_m^{n,n+1})) = -\frac{1}{\Lambda(\boldsymbol{v})}\left(\mathbb{E}(I_{kin}(\frac{\boldsymbol{u}_m^{n+1}-\boldsymbol{u}_m^n}{\tau})) + \mathbb{E}(I_{conv}(\boldsymbol{u}_m^{n+1/2})) + \mathbb{E}(I_{visc}(\boldsymbol{u}_m^{n+1/2}))\right) .$$

We now compute separately each term by setting $\boldsymbol{u}_m^n = \boldsymbol{u}_h^n + \boldsymbol{\varepsilon}^n$. First, from identities (4.4) it follows directly that

$$\mathbb{E}(I_{kin}(\frac{\boldsymbol{u}_m^{n+1}-\boldsymbol{u}_m^n}{\tau})) = I_{kin}(\frac{\boldsymbol{u}_h^{n+1}-\boldsymbol{u}_h^n}{\tau}), \quad \mathbb{E}(I_{visc}(\boldsymbol{u}_m^{n+1/2})) = I_{visc}(\boldsymbol{u}_h^{n+1/2}).$$

while the convective term requires a more careful treatment. First, notice that the following identity holds:

$$\mathbb{E}((\boldsymbol{\varepsilon}_{\text{i}}^n)^2) = \sigma^2 \sum_{\ell} (N_\ell)^2 = \sigma^2 \alpha \ , \quad \forall\ \text{i} = 1, \dots, \text{d},$$

with $\boldsymbol{\varepsilon}_{\text{i}}^n \in \mathcal{P}_h^1$ denoting the i-th spatial component of the vector $\boldsymbol{\varepsilon}^n \in [\mathcal{P}_h^1]^{\text{d}}$, and $N_\ell(\boldsymbol{x})$ the finite element shape function for the ℓ-th degree-of-freedom of $\mathcal{P}_h^1$. Therefore, also using identities (4.4) (and the Einstein summation convention) we proceed as follows:

$$\begin{aligned}
\mathbb{E}(I_{conv}(\boldsymbol{u}_m^n)) &= I_{conv}(\boldsymbol{u}_h^n) - \rho \int_\Omega \mathbb{E}((\boldsymbol{\varepsilon}^n \cdot \boldsymbol{\nabla}\boldsymbol{v}) \cdot \boldsymbol{\varepsilon}^n) + \rho \int_\Gamma \mathbb{E}((\boldsymbol{\varepsilon}^n \cdot \boldsymbol{n})(\boldsymbol{\varepsilon}^n \cdot \boldsymbol{v})) \\
&= I_{conv}(\boldsymbol{u}_h^n) - \rho \int_\Omega \mathbb{E}\left(\boldsymbol{\varepsilon}_{\text{i}}^n \frac{\partial \boldsymbol{v}_{\text{i}}}{\partial x_j} \boldsymbol{\varepsilon}_j^n\right) + \rho \int_\Gamma \mathbb{E}(\boldsymbol{\varepsilon}_{\text{i}}^n \boldsymbol{n}_{\text{i}} \boldsymbol{\varepsilon}_j^n \boldsymbol{v}_j) \\
&= I_{conv}(\boldsymbol{u}_h^n) - \rho \int_\Omega \mathbb{E}\left((\boldsymbol{\varepsilon}_{\text{i}}^n)^2\right) \frac{\partial \boldsymbol{v}_{\text{i}}}{\partial x_{\text{i}}} + \rho \int_\Gamma \mathbb{E}\left((\boldsymbol{\varepsilon}_{\text{i}}^n)^2\right) \boldsymbol{n}_{\text{i}} \boldsymbol{v}_{\text{i}} \\
&= I_{conv}(\boldsymbol{u}_h^n) - \rho\sigma^2 \int_\Omega \alpha\, \boldsymbol{\nabla} \cdot \boldsymbol{v} + \rho\sigma^2 \int_\Gamma \alpha \boldsymbol{v} \cdot \boldsymbol{n}
\end{aligned}$$

Therefore, the IMRP estimator bias can be written as:

$$\mathbb{E}(\delta p_{\text{imrp}}^{n+1/2}(\boldsymbol{u}_m^{n,n+1})) - \delta p_{\text{imrp}}^{n+1/2}(\boldsymbol{u}_h^{n,n+1}) = \frac{\rho\sigma^2}{2\Lambda(\boldsymbol{v})} B_{\text{imrp}}(\boldsymbol{v}) \tag{5.9}$$

with

$$B_{\text{imrp}}(\boldsymbol{v}) = -\int_\Omega \alpha\, \boldsymbol{\nabla} \cdot \boldsymbol{v} + \int_\Gamma \alpha \boldsymbol{v} \cdot \boldsymbol{n}.$$

We want to remark that this expression provides a closed form for the bias, and it is independent of the real velocity field and of the measurements. Therefore, it can be always

evaluated a priori. In fact, in the numerical examples we will verify that the bias is absolutely negligible with respect to the relative pressure, which is due to two reasons. Firstly, $\boldsymbol{\nabla} \cdot \boldsymbol{v}$ is (numerically) zero. Secondly, for example in the case of B-IMRP we have

$$B_{\text{imrp}}(\boldsymbol{v}) = -\int_{\Omega} \alpha\, \boldsymbol{\nabla} \cdot \boldsymbol{v} - \int_{\Gamma_{\text{i}}} \alpha + \frac{|\Gamma_{\text{i}}|}{|\Gamma_o|} \int_{\Gamma_o} \alpha.$$

However, it holds that

$$\int_{\Gamma} \alpha = \sum_{K} \int_{\Gamma_K} \alpha|_K = \sum_{K} |\Gamma_K| \int_{\Gamma_{\text{ref}}} \hat{\alpha}|_K$$

with Γ_{ref} a reference surface element and $\hat{\alpha}|_K$ the transformation of $\alpha|_K$ into the local coordinates of Γ_{ref}. Note that, by construction of the shape functions, $\hat{\alpha}|_K = \hat{\alpha}$ are the same for all K, so that the boundary terms in $B_{\text{imrp}}(\boldsymbol{v})$ cancel out.

Chapter 6

Numerical examples

6.1 Forward simulations

The synthetic measurements are obtained from a forward simulation in a stenotic tube where inlet and outlet width are set to $R = 2$cm, see Figure 6.1. We consider a Dirichlet boundary condition on Γ_{i} with a transient Womersley solution

$$u_{\text{in}}(x) = \sum_{k=0}^{N_W-1} \left(\frac{4a\left((2k+1)^2\sigma_{\boldsymbol{\varepsilon}} \sin(\omega t) - \omega\cos(\omega t)\right)}{\pi(2k+1)((2k+1)^4\sigma_{\boldsymbol{\varepsilon}}^2+\omega^2)} + \omega \mathrm{e}^{-(2k+1)^2\sigma_{\boldsymbol{\varepsilon}} t} \right) \sin\left((2k+1)\pi\tfrac{x-x_{min}}{R}\right),$$

with $a = \frac{P_{\text{drop}}}{\rho L}$, $\sigma_{\boldsymbol{\varepsilon}} = \frac{\mu\pi^2}{4\rho\left(\frac{R}{2}\right)^2}$, $N_W = 50$, L the length between the inlet and outlet of our geometry, and $P_{drop} = 1877$ bary, which was calibrated to obtain a peak flow rate of 333 cc/s at 200 ms without any stenosis, i.e. a straight tube. The frequency was chosen as $w = \frac{1}{400}\ \frac{1}{\text{ms}}$ in order to emulate a realistic cardiac output. Moreover, zero Neumann on Γ_o and non-slip Dirichlet on Γ_w boundary conditions imposed. The physical parameters were chosen as $\mu = 0.035$ Poise and $\rho = 1.0$ gr/cm^3.

The numerical solution of the reference problem was performed using a monolithic velocity-pressure coupling. The space-semidiscretization was performed via standard inf-sup stable linear+bubble finite elements for the velocity, and linear for the pressure [13] with a mesh size of 0.5 mm. A backward Euler scheme was used for the time-semidiscretization with time-step of 5 ms, with a semi-implicit treatment of the convective term, and we include a Temam stabilization term to ensure Lyapunov stability of the solution in time [15]. At that spatial refinement level, no volume or backflow convective instabilities were observed, so no volume convective or backflow stabilization terms were included in order to not perturb the original equation, so no SUPG [16] or backflow stabilization [17] were necessary.

6.2 Synthetic measurements

We generated synthetic measurements (see Figure 6.1) considering the following perturbations of the data:

- We consider consider additive Gaussian noise [18]. Standard deviation was chosen as 10% of the peak velocity as it is usually done in clinical Phase-Contrast imaging adjusting the expected peak velocity (called *VENC* parameter) [6].
- We considered realistic time subsampling of 20ms, and also using no temporal subsampling for the sake of comparison.
- We considered spatial subsampling of 1mm, 2mm and 3mm.

6.3 Weighting functions for IMRP

As introduced in Section 5.2, we will use two types of testing functions with the IMRP: A Poiseuille flow (Problem (5.7)), called P-IMRP; and a Brinkman flow (Problem (5.8)), called B-IMRP. For the B-IMRP flow, we used a viscosity value of $\nu = \mu = 0.035$ for a simulation and another value of $\nu = 10^{-4} \cdot 0.035$ for another, in order to make it more strongly differ from the P-IMRP flow. In Figure 6.2 we can see P-IMRP and B-IMRP with $\nu = \mu = 0.035$.

6.4 Estimation results: noise-free measurements

We investigate first the sensitivity of the results to the spatial subsampling of the measurements.

Note that the best methods turn out finally to be the P-IMRP, B-IMRP and STEint methods. These are then assessed and compared with noisy measurements.

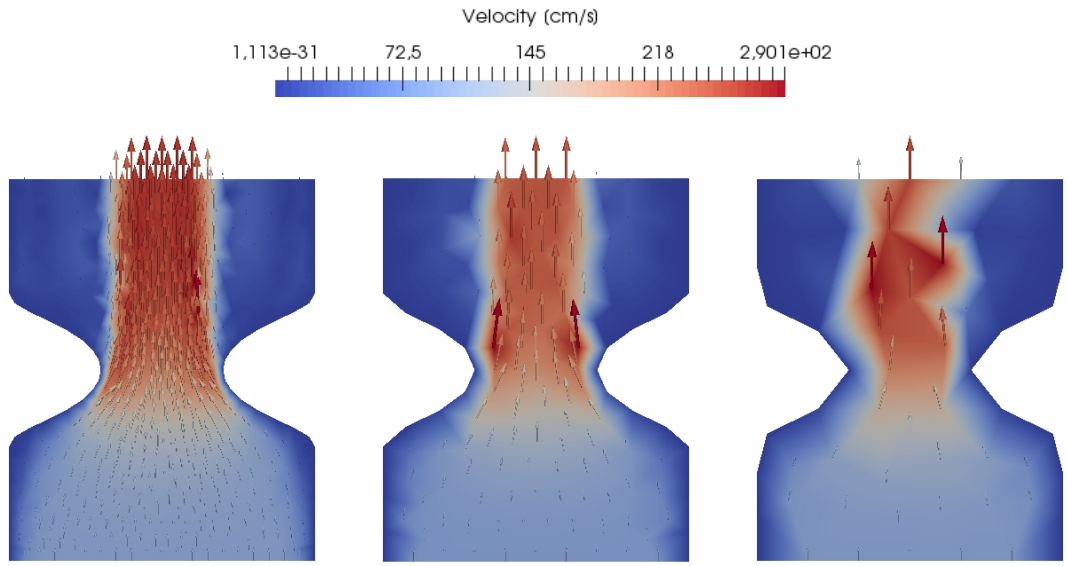

(b) No noise - $h = 1$ mm (c) No noise - $h = 2$ mm (d) No noise - $h = 3$ mm

(e) 10% noise - $h = 1$ mm (f) 10% noise - $h = 2$ mm (g) 10% noise - $h = 3$ mm

Figure 6.1: Spatially subsampled measurements with and without noise at time t=0.2 seconds.

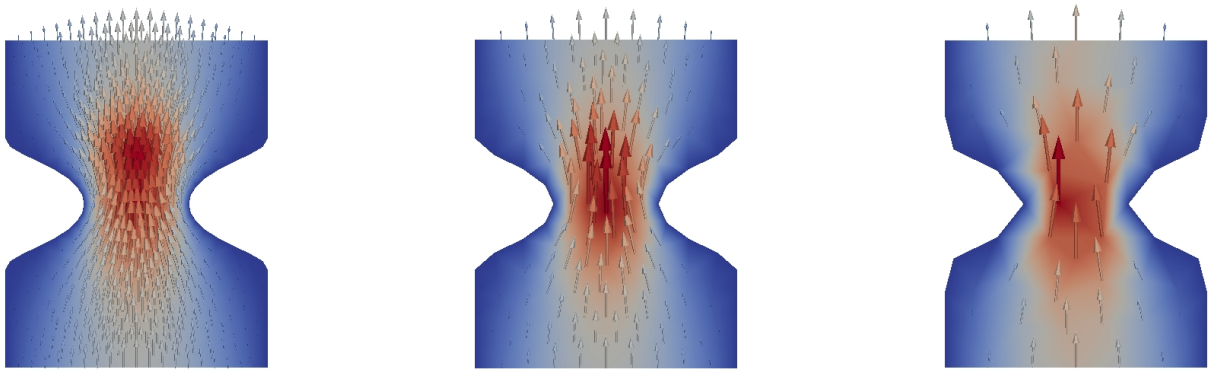

(a) P-IMRP - h=1mm (b) P-IMRP - h=2mm (c) P-IMRP - h=3mm

(d) B-IMRP - h=1mm (e) B-IMRP - h=2mm (f) B-IMRP - h=3mm

Figure 6.2: Test functions for IRMP for different spatial resolutions

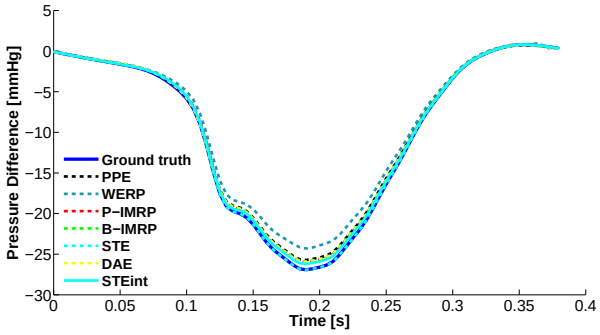

(a) Best methods: $h = 0.5$

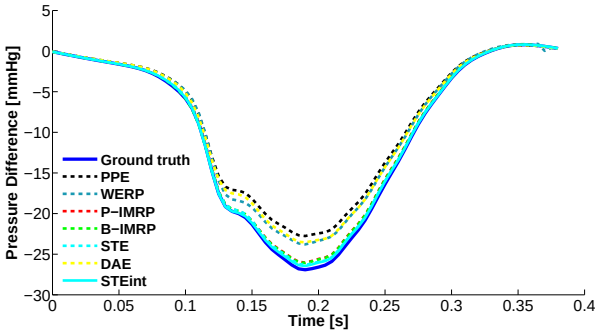

(b) Best methods: $h = 1$

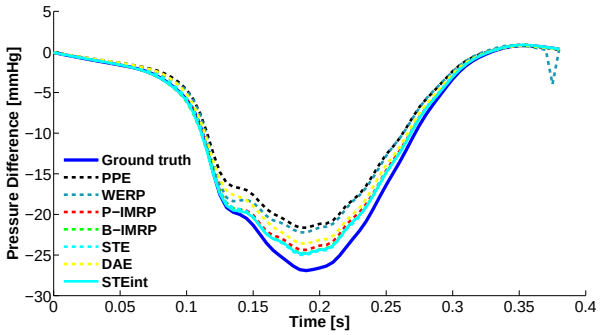

(c) Best methods: $h = 2$

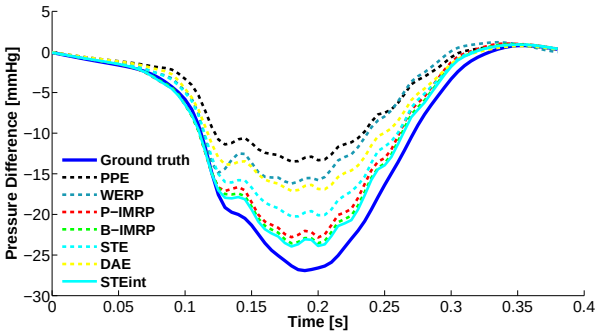

(d) Best methods: $h = 3$

Figure 6.3: Noise-free estimations for best methods.

6.5 Estimation results: noisy measurements

We performed the same study but including a 10% noise, meaning that the standard deviation was chosen as $\sigma = 0.1 \cdot \max_n(\|\boldsymbol{u}_m^n\|_{\ell^\infty})$. We use 100 noise samples, and we present the mean pressure curves in Figure 6.4, the standard deviations for peak pressure in Figure 6.5(a) and the mean preassure error with respect to the ground truth at peak pressure time in Figure 6.5(b). Note that the standard deviation of the pressure estimations diminishes linearly with the spatial discretization size h for all methods. These values are similar, except for the WERP, which has around twice the standard deviation as the best methods (IMRP and STEint). From Figure 6.5(b), the methods with the smallest errors in the mean relative pressures are STEint, B-IMRP and P-IMRP.

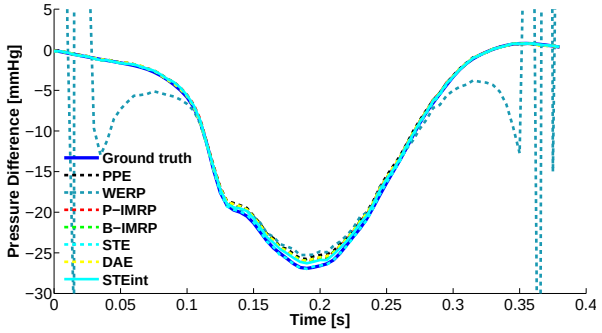

(a) Best Methods: $h = 0.5$

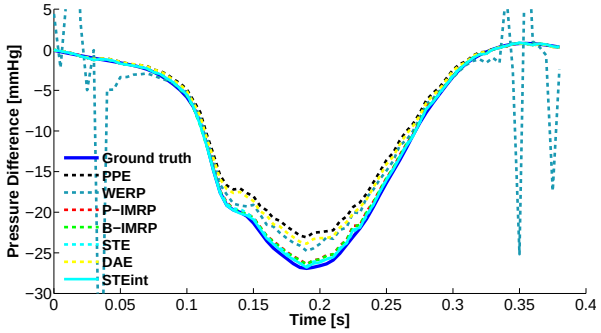

(b) Best Methods: $h = 1$

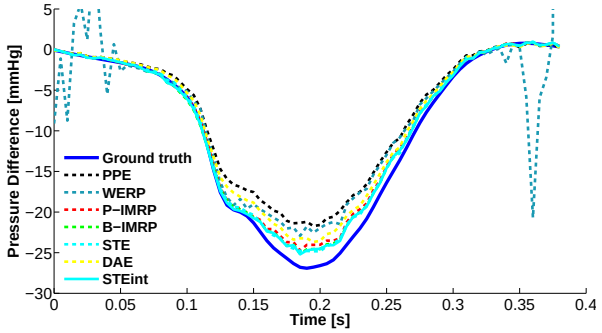

(c) Best Methods: $h = 2$

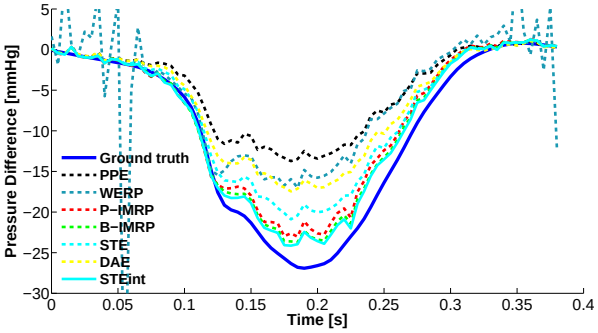

(d) Best Methods: $h = 3$

Figure 6.4: Mean estimations with 10% noise for best methods.

Moreover, we verify that the WERP and c-WERP are unstable for small flows, and that the the c-WERP reduces the bias of the estimator when we compare for the original fine mesh of $h = 0.5$mm (Figure 6.6(a)). However, as we interpolated the velocity from P1b to P1 elements, an interpolation error induces an underestimation of δp . By chance, with the overestimation from noise, this underestimation makes WERP closer to ground truth than c-WERP (Figure 6.6(b)).

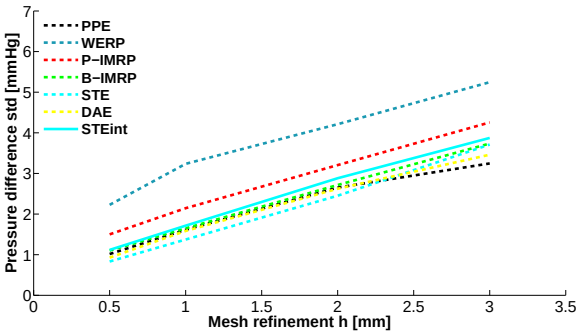

(a) Standard deviation

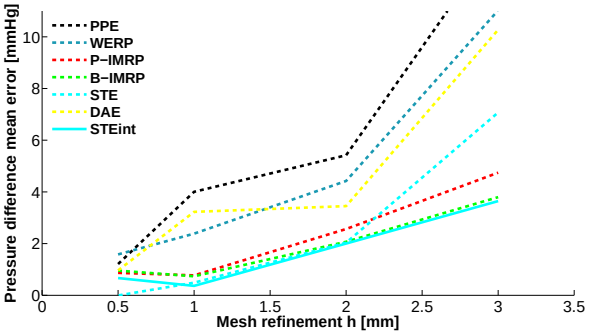

(b) Mean error

Figure 6.5: Standard deviation and mean error estimations with 10% noise and $\tau = 5$ms for best methods for different mesh refinement.

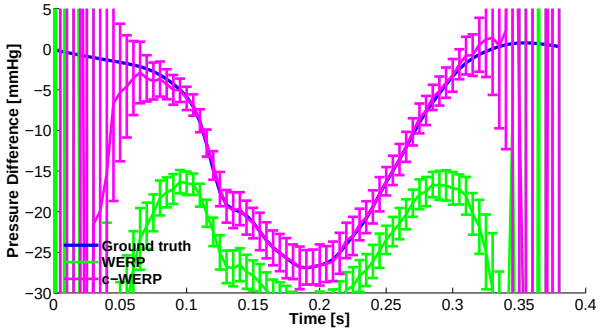

(a) $h = 0.5$ - Fine mesh using elements P1b

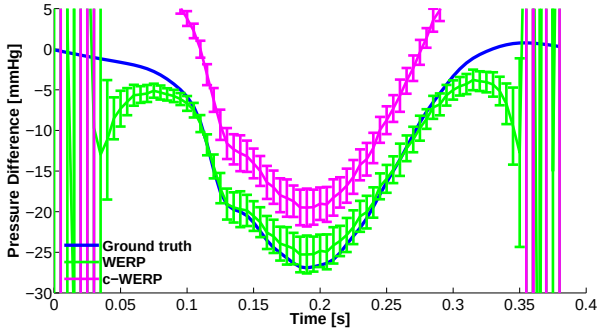

(b) $h = 0.5$ - Fine mesh using elemrnts P1 interpolated from P1b

Figure 6.6: Correction effect for c-WERP in fine and coarse meshes.

6.6 Estimation results: sensitivity to time subsampling (including noise)

In Figure 6.7 we present methods B-IMRP and STEint with $\tau = 20$ms. The first we can remark is that the time subsampling do not have a relevant impact on the estimation. Moreover, note that at the beginning and end of the cycle the estimator variance is smaller than at peak pressure. This can be explained as follows: the dominating term at low Reynolds numbers is the kinetic, and it's variance is inversely proportional to $1/\tau^2$. This can be verified when we split the different terms of the pressure gradient for the IMRP and analyze their variances independently, see Figure 6.8 for an analysis of B-IMRP. We can also see that viscous contribution is negligible in this geometry.

In Figure 6.9(a) and 6.9(b) we see that time undersampling does not change results in a significant way.

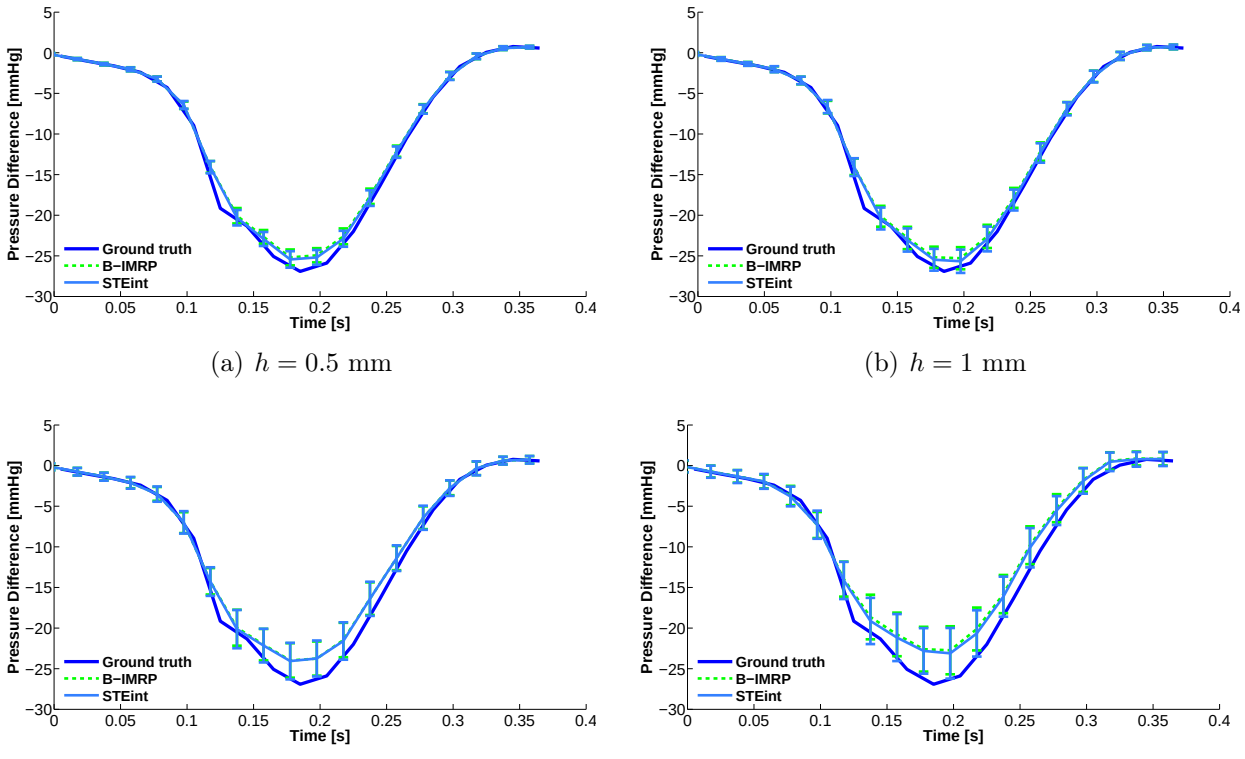

(a) $h = 0.5$ mm

(b) $h = 1$ mm

(c) $h = 2$ mm

(d) $h = 3$ mm

Figure 6.7: Mean estimations with 10% noise and 20 ms for B-IMRP and STEint.

6.7 Estimation results for a severe coarctation

A more severe coarctation could induce a greater viscous contribution for IMRP methods, but as it is shown in Figure 6.11, the viscous term grows but it is still negligible with respect to advection and kinetic terms. Note that to estimate peak pressure difference with B-IMRP,

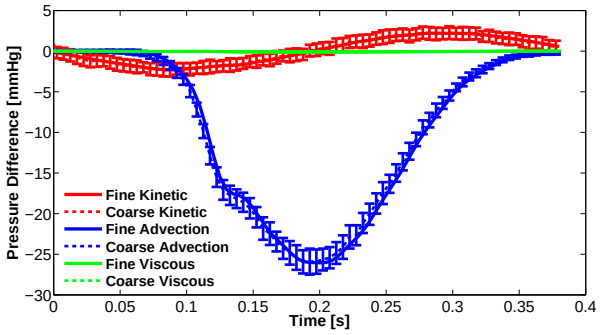

(a) $h = 1\text{mm}$, $\tau = 5\text{ms}$

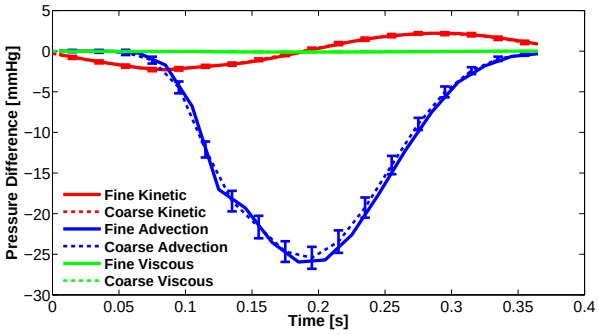

(b) $h = 1\text{mm}$, $\tau = 20\text{ms}$

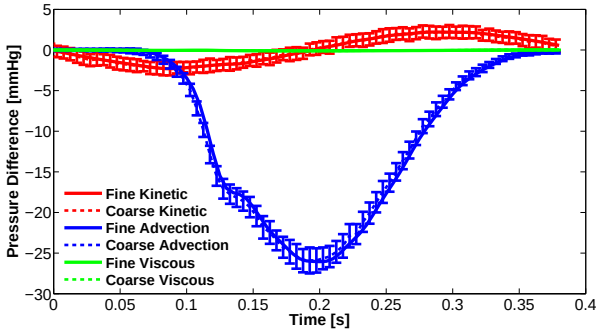

(c) $h = 2\text{mm}$, $\tau = 5\text{ms}$

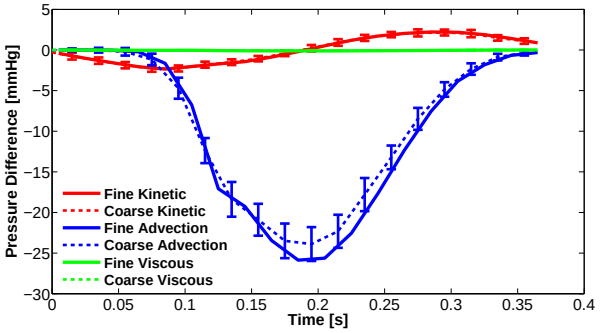

(d) $h = 2\text{mm}$, $\tau = 20\text{ms}$

Figure 6.8: Comparison between B-IMRP integral terms contribution for $h = 1, 2\text{mm}$, $\tau = 5, 20\text{ms}$, 10% noise, for 60% coarctation.

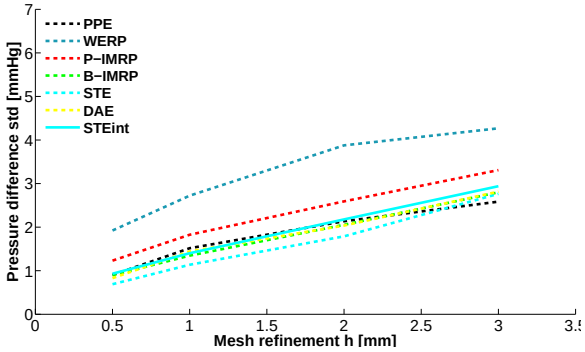

(a) Standard deviation

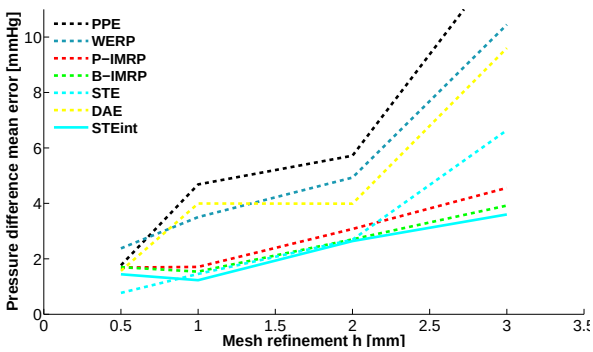

(b) Mean error

Figure 6.9: Standard deviation and mean error estimations with 10% noise and $\tau = 20\text{ms}$ for best methods for different mesh refinement with 60% coarctation.

for this example we only care about the convective term, since both kinetic term and viscous terms are negligible.

In Figure 6.10, we show pressure estimation for the best methods. We can see that at 70% coarctation, pressure difference grows rapidly to ~ 55 mmHg, and Figure 6.12(a) shows us that standard deviation grows for every method, but B-IMRP and STEint still being among the best estimators. They also keep having the the smallest error in the mean in Figure 6.12(b).

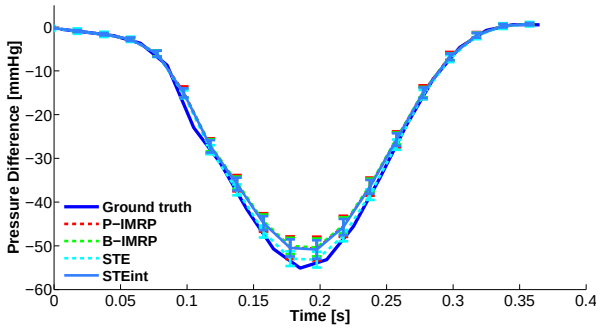

(a) Best methods: $h = 0.5$

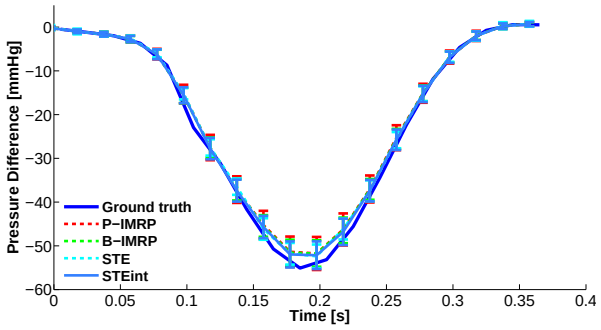

(b) Best methods: $h = 1$

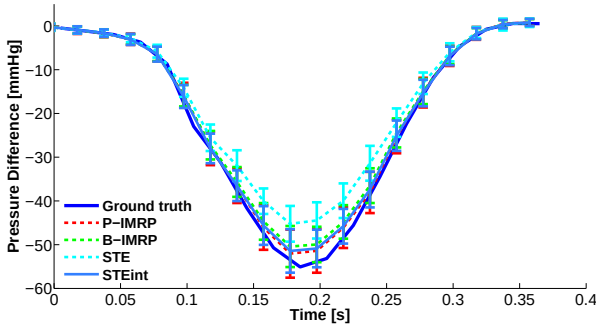

(c) Best methods: $h = 2$

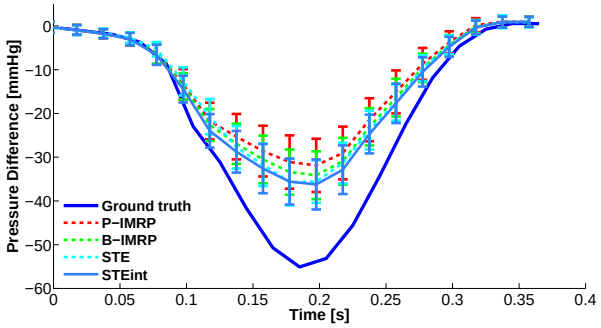

(d) Best methods: $h = 3$

Figure 6.10: Mean estimations for best methods with 10% noise and 20 ms for a 70% coarctation.

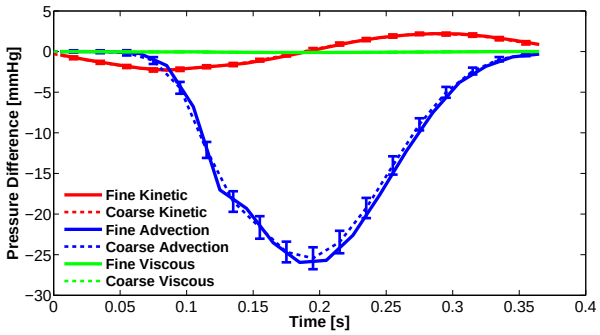

(a) Integral terms contribution for 60% coarctation

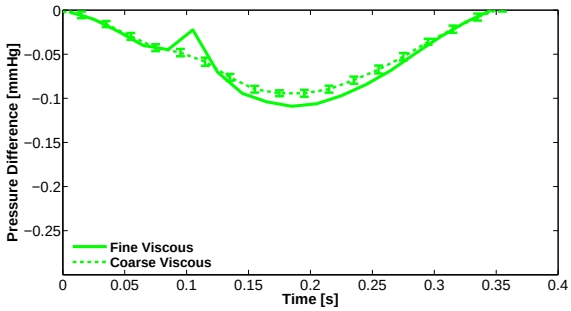

(b) Zoom for integral terms contribution for 60% coarctation

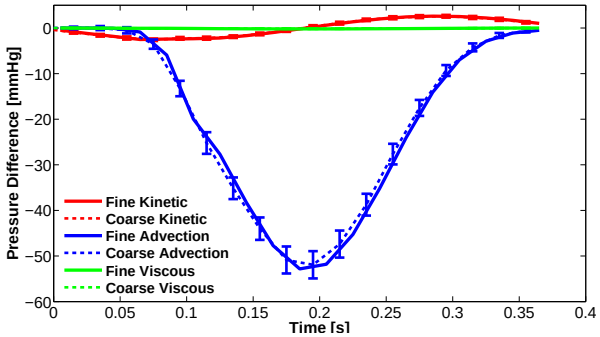

(c) Integral terms contribution for 70% coarctation

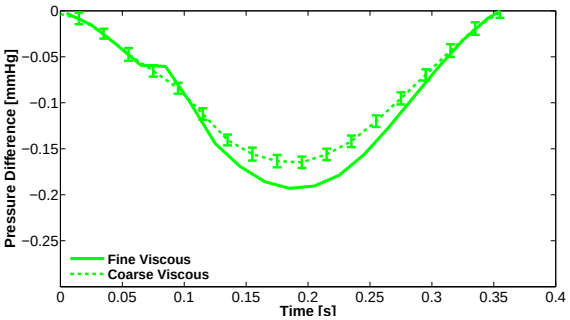

(d) Zoom for integral terms contribution for 70% coarctation

Figure 6.11: Comparison between B-IMRP integral terms contribution for $h = 1$mm, $\tau = 20$ms, 10% noise, for 60% and 70% coarctations.

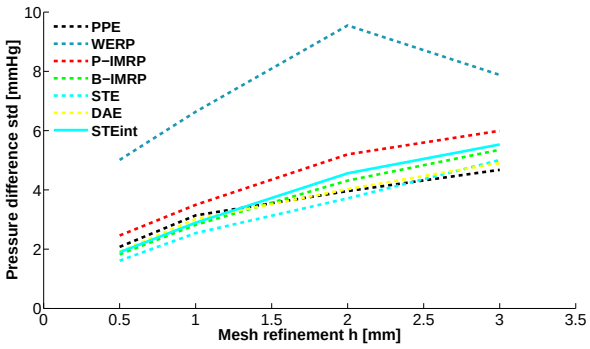

(a) Standard deviation

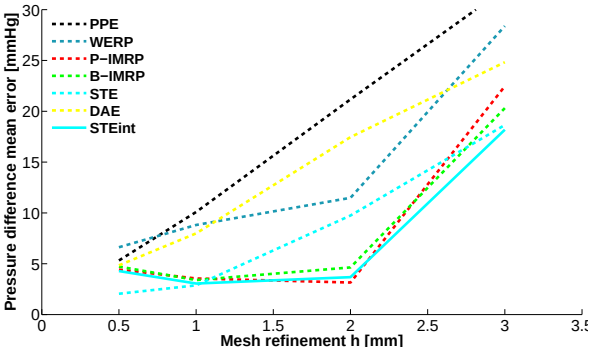

(b) Mean error

Figure 6.12: Standard deviation and mean error estimations with 10% noise and $\tau = 20$ms for best methods for different mesh refinement with 70% coarctation.

Chapter 7

Discussion and perspectives

PPE for an aortic coarctation was introduced in [9]. The authors tested this method with a 3D tube and with a 3D aortic geometry without any coarctation. In [11], the authors proposed WERP and compared it with Simplified Bernoulli, Unsteady Bernoulli and PPE methods, using an aortic geometry with a small coarctation. In [10], they propose STE and compared it with PPE, showing a great superiority in terms of error with noise of 0%, 5% and 10%.

In this work, we detect a systematic noise bias for WERP, that was not considered in [9] but was visible in Figure 7 of [9]. In addition, we propose a correction c-WERP that fixes WERP's bias. We proposed a new method called IMRP, improving robustness respect to noise and mesh coarseness. Also we complement [10] by proposing a natural modification to STE: integrating by parts the second derivatives in space and reducing derivation order. In Table 7.1 we have a summary of the most important methods for this work.

Ranking	Method	Estimation	Computational cost	Mean error	Std of the error
1	B-IMRP	δp	1	1	1
1	P-IMRP	δp	1	1	1
1	STEint	$p \in \Omega$	2	1	1
2	STE	$p \in \Omega$	2	2	1
3	WERP	δp	1	3	2
4	PPE	$p \in \Omega$	2	4	1

Table 7.1: Summary of the most important methods. "Estimation" column tells where if we obtain pressure over the whole domain ($p \in \Omega$) or just a difference of pressure between two surfaces (δp). "Computational cost", "Mean error" and "Std of the error" columns divide methods in categories, being 1 the one with best performance. In the same way, we propose a global ranking for pressure estimation methods.

In this work we found a number of modifications for the pressure estimation algorithms which, generally, improves the methods.

- Integrate by parts to reduce derivation orders and noise amplification.
- Use noise-free auxiliary functions, different from measurements, to reduce estimator's

variance and bias.

- Approximate velocity in time $t = (n + \frac{1}{2})\tau$, where τ is the time step, with a scheme $\boldsymbol{u}^{n+\frac{1}{2}} = \frac{\boldsymbol{u}^{n+1}+\boldsymbol{u}^{n}}{2}$, this reduces estimator's variance.

We verify that c-WERP corrects well WERP's bias when we don't have numerical error due to spatial resolution, but still it has a significantly large variance. This makes WERP and c-WERP unaccurate compared to other methods.

Time subsampling does not induce major problems to pressure estimation. With a time step of $\tau = 20$ ms we obtain comparable results to $\tau = 5$ ms. Having a bigger τ even reduces variance where the kinetic contribution is greater. Unfortunately, peak pressure difference is calculated when fluid aceleration is negligible (i.e. $\frac{\boldsymbol{u}^{n+1}-\boldsymbol{u}^{n}}{\tau} \approx 0$), so the kinetic term is also negligible. Then, peak pressure difference variance is not reduced by taking a bigger time step.

With a greater coarctation we obtain the same conclusions, the only difference is that peak preassure difference is greater. Viscous term contributes more as coarctation level grows, but it is still negligible.

We determine that among all these methods, B-IMRP and STEint are the most robust options with respect to space, time undersampling and noise, as we can see in Figure 6.7. B-IMRP is much faster to compute (since it need only one mixed problem solution), but it gives us a peak pressure difference estimation between only two points. On the other hand, STEint is more expensive computationaly but it gives a preassure estimation in the whole geometry. This can be used later to obtain more relevant information in the future.

Another important contribution of this work is the systematic benchmark for noise and spatial resolution. We show that for a fixed noise level, the pressure estimation improves as h decreases.

Some future extensions of this work could be:

- Test this methods in 3D with synthetic data and then with real 4D flow measurements.
- Quantify estimators variance for any given geometry, space step h and measurements variance.
- Study in a theoretical way why there is a consistent pressure difference underestimation as our mesh is coarser.

Bibliography

[1] Warnes CA, Williams RG, Bashore TM, Child JS, Connolly HM, Dearani JA, del Nido P, Fasules JW, Graham TP, Hijazi ZM, *et al.*. ACC/AHA 2008 guidelines for the management of adults with congenital heart disease. *Journal of the American College of Cardiology* 2008; **52**(23):e143–e263.

[2] Mendelsohn AM, Lloyd TR, Crowley DC, Sandhu SK, Kocis KC, Beekman RH. Late follow-up of balloon angioplasty in children with a native coarctation of the aorta. *The American journal of cardiology* 1994; **74**(7):696–700.

[3] Presbitero P, Demarie D, Villani M, Perinetto EA, Riva G, Orzan F, Bobbio M, Morea M, Brusca A. Long term results (15-30 years) of surgical repair of aortic coarctation. *British heart journal* 1987; **57**(5):462–467.

[4] Vahanian A, Alfieri O, Andreotti F, Antunes MJ, Barón-Esquivias G, Baumgartner H, Borger MA, Carrel TP, De Bonis M, Evangelista A, *et al.*. Guidelines on the management of valvular heart disease (version 2012). *European Heart Journal* 2012; **33**(19):2451–2496, doi:10.1093/eurheartj/ehs109. URL `http://eurheartj.oxfordjournals.org/content/33/19/2451`.

[5] Markl M, Frydrychowicz A, Kozerke S, Hope M, Wieben O. 4D flow MRI. *Journal of Magnetic Resonance Imaging* 2012; **36**(5):1015–1036.

[6] Dyverfeldt P, Bissell M, Barker AJ, Bolger AF, Carlhäll CJ, Ebbers T, Francios CJ, Frydrychowicz A, Geiger J, Giese D, *et al.*. 4D flow cardiovascular magnetic resonance consensus statement. *Journal of Cardiovascular Magnetic Resonance* 2015; **17**(1):1–19.

[7] Ebbers T, Wigström L, Bolger AF, Engvall J, Karlsson M. Estimation of relative cardiovascular pressures using time-resolved three-dimensional phase contrast MRI. *Magnetic resonance in medicine* 2001; **45**(5):872–879.

[8] Ebbers T, Farnebäck G. Improving computation of cardiovascular relative pressure fields from velocity MRI. *Journal of Magnetic Resonance Imaging* 2009; **30**(1):54–61.

[9] Krittian SB, Lamata P, Michler C, Nordsletten DA, Bock J, Bradley CP, Pitcher A, Kilner PJ, Markl M, Smith NP. A finite-element approach to the direct computation of relative cardiovascular pressure from time-resolved MR velocity data. *Medical image analysis* 2012; **16**(5):1029–1037.

[10] Švihlová H, Hron J, Málek J, Rajagopal K, Rajagopal K. Determination of pressure data from velocity data with a view toward its application in cardiovascular mechanics. Part 1. Theoretical considerations. *International Journal of Engineering Science* 2016, In press; URL `http://www.sciencedirect.com/science/article/pii/S0020722515001858`.

[11] Donati F, Figueroa CA, Smith NP, Lamata P, Nordsletten DA. Non-invasive pressure difference estimation from PC-MRI using the work-energy equation. *Medical Image Analysis* 2015; **26**(1):159–172.

[12] Lamata P, Pitcher A, Krittian S, Nordsletten D, Bissell MM, Cassar T, Barker AJ, Markl M, Neubauer S, Smith NP. Aortic relative pressure components derived from four-dimensional flow cardiovascular magnetic resonance. *Magnetic resonance in medicine* 2014; **72**(4):1162–1169.

[13] Girault V, Raviart PA. *Finite element methods for Navier-Stokes equations: theory and algorithms*, vol. 5. Springer Science & Business Media, 2012.

[14] Scott L, Vogelius M. Norm estimates for a maximal right inverse of the divergence operator in spaces of piecewise polynomials. *RAIRO-Modélisation mathématique et analyse numérique* 1985; **19**(1):111–143.

[15] Temam R. Une méthode d'approximation de la solution des équations de navier-stokes. *Bulletin de la Société Mathématique de France* 1968; **96**:115–152.

[16] Brooks AN, Hughes TJ. Streamline upwind/Petrov-Galerkin formulations for convection dominated flows with particular emphasis on the incompressible Navier-Stokes equations. *Computer methods in applied mechanics and engineering* 1982; **32**(1):199–259.

[17] Bertoglio C, Caiazzo A. A Stokes-residual backflow stabilization method applied to physiological flows. *Journal of Computational Physics* 2016; **313**:260–278.

[18] Bao P, Zhang L. Noise reduction for magnetic resonance images via adaptive multiscale products thresholding. *Medical Imaging, IEEE Transactions on* 2003; **22**(9):1089–1099.